FAILURE MECHANISMS OF PRESSURIZED MICROCHANNELS, MODEL AND EXPERIMENTS

M.T. Blom[1], N.R. Tas[1], G. Pandraud[1], E. Chmela[2], J.G.E. Gardeniers[1], R. Tijssen[2], M. Elwenspoek[1], A. van den Berg[1]
[1] MESA Research Institute, University of Twente, The Netherlands,
P.O. Box 217, 7500 AE Enschede, the Netherlands, e-mail: m.t.blom@el.utwente.nl
[2] Department of Chemical Engineering, University of Amsterdam, The Netherlands

ABSTRACT

Microchannels were created by fusion bonding of a Pyrex and a thermally oxidized silicon wafer. The maximum pressure which can be applied to these channels was investigated. In order to find the relation between this maximum pressure, channel geometry, materials elasticity and bond energy an energy model was developed. It was shown that the model is substantiated by the pressure data, from which it could be calculated that the effective bond energy increased from 0.018 J/m^2 to 0.19 J/m^2 for an annealing temperature ranging from 310^{0}C to 470^{0}C.

INTRODUCTION

High pressure microchannels can be useful for a number of applications, for instance high pressure separation techniques [1]. Of course, the maximum pressure such channels can withstand is an important parameter. Because microchannels often are fabricated using bonding of two wafers [1,2] the maximum pressure is directly related to the failure of either the bond or of one of the wafers. In this case we consider a microchannel fabricated by bonding of a silicon and a Pyrex wafer. As Pyrex is by far the weakest material of the two, there are two failure mechanisms for a pressurized microchannel. One mechanism is cracking of the Pyrex at the side of the channel, as is depicted in fig. 1A: the total of bending and shear stress exceeds the maximum stress the Pyrex can withstand and the Pyrex breaks.

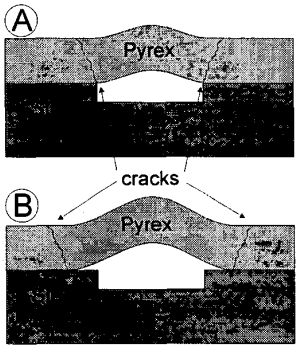

Figure 1: Channel failure mechanisms. With mechanism A only the Pyrex breaks, mechanism B implies that first the bond interface opens before the Pyrex cracks.

The second mechanism is shown in fig. 1B. If the pressure is large enough the bonding interface will open. Once that happens, the pressure acts on an increased area and the interface will open further. During this process the stress in the Pyrex will increase until it exceeds the maximum stress at some point in the material. Depending on the geometry, the material properties and the bond strength involved, either the glass wafer breaks first, due to mechanism A, or the Pyrex wafer peels off (B). In this work, we have focused on failure mode B. A theory relating geometry, material properties, maximum pressure and bond strength was developed.

In this model the bond strength is characterized by the effective bonding energy, which is defined as the separation energy per unit apparent contact area. For rough surfaces the effective bond energy $\Delta\gamma_b$ is lower than the work of adhesion $\Delta\gamma$ [3], because 1) the real contact area is smaller than 100%, 2) part of the work of adhesion is stored as elastic deformation energy needed to compress the higher asperities in contact. The work of adhesion is defined as the work needed to separate the contacting surfaces from full contact to infinity.

By applying the energy model to bonded samples that were annealed at different temperatures, the dependence of the bond energy on the annealing temperature could be investigated.

THEORY: ENERGY DESCRIPTION

The theory relating channel pressure, geometry, material properties and bond energy requires an energy balance. The total (free) energy for the situation of interest equals the sum of the elastic deformation energy, the surface energy and the hydraulic energy of the pressure source:

$$U_{tot}(x,y) = U_{elast}(x,y) + U_{surf}(x,y) - p\Delta V(x,y) \quad (1)$$

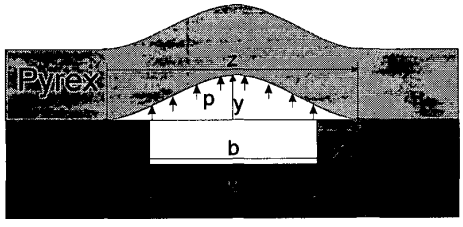

Figure 2: Channel geometry. The distance across which the Pyrex is deflected b is related to the detachment length x and the actual channel width w as $b = 2x + w$. Also shown are the channel center deflection y, the pressure p and the distance across the channel from one detached side called z.

In this expression ΔV is the volume change due to deflection of the Pyrex wafer, p is the applied pressure, x is the detachment length and y the channel center deflection (fig. 2). A stable equilibrium is obtained for a minimum in the total energy for variation of x and y, which gives the situation we want to describe.

Elastic deformation energy per unit channel length

We start the calculation of the bending energy of the Pyrex by considering the cross-section of the channel as a beam that is rigidly clamped on both sides, and loaded with a uniform pressure p (fig. 2).
For a beam of length b, modulus of elasticity E and moment of inertia I, the elastic deformation energy per unit channel length L is given by [5]:

$$U_{elast} = \frac{EI}{2L}\int_0^b \left(\frac{d^2v(z)}{dz^2}\right)^2 dz \qquad (2)$$

in which $v(z)$ is the deflection of the beam at a position z along the beam and b the distance across which the Pyrex is deflected (fig. 2). The deformation $v(z)$ of a beam rigidly clamped on both sides and loaded with uniform pressure $p' = p$ x *beam width* is given by [5]:

$$v(z) = \frac{p' z^2 (b-z)^2}{24EI} \qquad (3)$$

We have to express this in the internal variable y. This can be done by identifying that the maximum deflection $v_{max} = y$ occurs at $z = \frac{1}{2}b$. Thus $v(z)$ can be written as a function of y:

$$v(z) = \frac{16yz^2}{b^4}(b^2 - 2bz + z^2) \qquad (4)$$

With the moment of inertia $I = {}^1/_{12}\, L\, t^3$, where t is the thickness of the Pyrex wafer, it follows that:

$$U_{elast}(x,y) = \frac{EI}{2L}\int_0^b \left(\frac{d^2v(z)}{dz^2}\right)^2 dz = \frac{128}{15}\frac{Et^3}{b^3}y^2 \qquad (5)$$

Surface energy per unit channel length

The energy per unit channel length needed to open the bonding interface by a distance x (on both sides) is given by the effective bond energy $\Delta\gamma_b$ multiplied with the exposed area $2x$:

$$E_{surf}(x,y) = 2x\Delta\gamma_b \qquad (6)$$

Hydraulic energy per unit channel length

The volume change determining the hydraulic energy can be calculated by integrating expression (4) along the beam and multiplying with the channel length L. The hydraulic energy per unit channel length is then:

$$U_{hydraulic}(x,y) = p\Delta V(x,y) = \tfrac{8}{15}pyb \qquad (7)$$

Total energy

For a stable situation, expression (1) for the total energy $U_{tot}(x,y)$ should be minimized for variation of x and y. For y this means:

$$\frac{\partial U_{tot}(x,y)}{\partial y} = 0 \qquad (8)$$

giving an expression for the channel center deflection y as a function of geometry, material constants and the pressure.

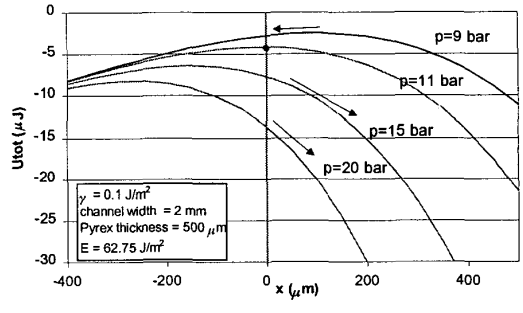

Figure 3: The total energy as a function of the detachment length. It is clear that for pressures below 11 bar a local equilibrium exists because $x > 0$. For higher pressures, no equilibrium exists, therefore x must increase and the bond opens.

The result corresponds to ref. [5]. Substituting this in the expression for the total energy gives $U_{tot}(x)$. The resulting total energy $U_{tot}(x)$ as a function of the detachment length x (fig. 2) is shown in fig. 3 for different pressures.

Initially, $x = 0$ (refer to fig. 3). For a relatively low pressure $p = 9$ bar, a local energy minimum is obtained at $x = 0$, because the function is bound by the condition that $x \geq 0$. At $p = 11$ bar, the situation is on the verge of becoming unstable. For a further increase in the pressure no minimum in the total energy can be found. This results in an increase of x, implying that the bond interface is opened.

From fig. 3 it can be concluded, that the point where the interface starts to open can be described by $x = 0$ and:

$$\frac{\partial U_{tot}(x,y)}{\partial x} = 0 \qquad (9)$$

Combining expressions (8) and (9) for $x = 0$ gives the requested pressure behaviour as a function of geometry, material parameters and effective bond energy:

$$p = \sqrt{\frac{2048 E t^3 \Delta\gamma_b}{77}} \frac{1}{w^2} \qquad 10)$$

in which w is the actual channel width (fig. 2). Thus, according to this model the critical pressure increases linearly with $1 / w^2$. In a plot of the maximum pressures against the reciprocal of the squared channel width, the effective bond energy can be extracted from the tangent. For individual measurements the expression above can be rewritten for the effective bond energy as a function of channel width and pressure:

$$\Delta\gamma_b = \frac{77}{2048} \frac{w^4 p^2}{E t^3} \qquad (11)$$

FABRICATION OF THE TEST STRUCTURES

Principally, the channels were etched into a 4" silicon wafer and closed by bonding a 3" Pyrex wafer on top.

At first, a 160 nm low-stress silicon nitride layer was deposited on a 4" (100) silicon wafer and patterned with Reactive Ion Etching using a CHF_3/O_2 mixture. Subsequently, the wafers were etched in a 25 wt % KOH solution at 75°C for 302 minutes, giving an etch depth of approximately 310 µm. After cleaning and stripping the nitride mask layer, a 1 µm wet silicon oxide layer was thermally grown at 1150°C.

The Pyrex wafer was polished for 5 minutes using a SemiSpur 25 polishing solution. After cleaning both the silicon and the Pyrex wafer, they were contacted and a prebond was formed. Four wafer pairs were annealed

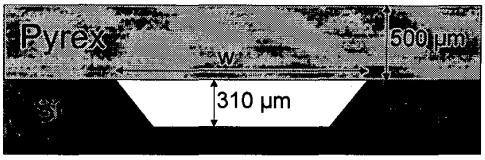

Figure 4: Channel cross-section. The silicon is patterned using KOH-etching leaving an anisotropic etch profile.

for 2 hours at different temperatures: 316°C, 363°C, 425°C and 470°C. The annealing temperature is limited for practical reasons by the strain point of the Pyrex which is 510°C according to the manufacturer's (Corning) specification.

The channel height, given by the KOH etch depth is designed for the use of common capillaries with an outer diameter ranging from 260 µm to 300 µm. This gives a channel cross-section as shown in fig. 4.

The channel ends are adapted for use of the same capillaries as mentioned above. Therefore they are 560 µm wide, for a 6 mm distance on both sides (fig. 5). On a 4" wafer only 5 channels were created in order to leave sufficient bonding area. The channel widths are 560, 750, 1000, 1500, 2000 µm. The channels are linked by a thin (20 µm wide) channel to the outer world. This is done in order the release the pressure that would build up in the otherwise closed channels. The resulting mask structure is shown in fig. 5.

By sawing along the thin channel, the channels are opened. Before testing capillaries were glued into both channel ends, using epoxy glue cured at 100°C.

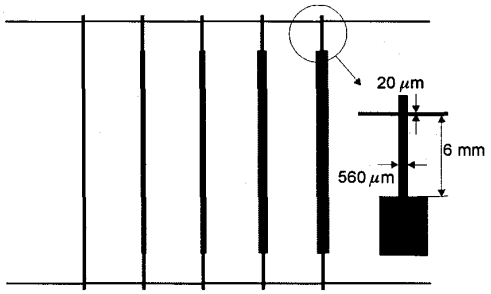

Figure 5: Mask structure. Five channels having different widths are made. The channel ends are adapted to facilitate insertion of glass capillaries.

Prior to bonding, the glass interface was characterized by AFM-measurements (fig. 6). This gives the possibility to estimate the real contact area in the bonded area. The roughness, elastic and adhesion parameters have been collected in table 1.

Using an elastic adhesive contact model [3,4] the normalized real contact area as a function of the dimensionless adhesion parameter θ can be found (fig. 7). This model is valid only under the assumption that

Table 1: Roughness, elastic and adhesion parameters of the contacting surfaces.

Asperity Density	η	4×10^{13} m^{-2}
Asperity Radius	R	2 μm
Work of Adhesion	$\Delta\gamma$	0.1 J·m^{-2}
SD Summit Level	σ	0.4 nm
Compliance	D	1.59×10^{-11} Pa^{-1}
RMS Roughness	σ_{RMS}	0.5 nm

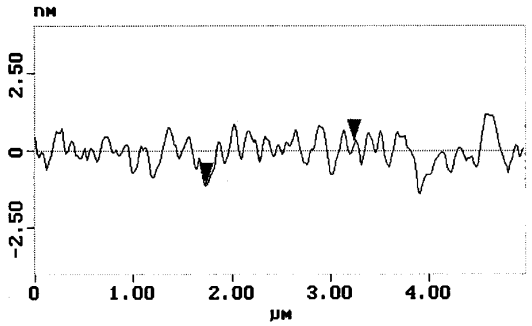

Figure 6: Cross-section of a Pyrex AFM-scan, from which the adhesion parameter can be calculated.

the deformation is elastic. From the Pyrex hardness it can be concluded that this assumption is justified. The normalized real contact area A^* is defined by [6,7]:

$$A^* = \frac{A_r}{\eta R \sigma A_a} \tag{12}$$

With A_r the real and A_a the apparent contact area. Using the measured parameters, A^*=30 corresponds to full contact. The adhesion parameter is defined by [8]:

$$\theta = \frac{\sigma^{3/2} R^{1/2}}{D \Delta\gamma R} \tag{13}$$

After pre-bonding the work of adhesion is expected to be 0.1 J/m^2 [9]. Assuming that the silicon wafer is perfectly smooth, and taking the parameters from table 1, it can be calculated that the adhesion parameter equals 3.6 and the relative real contact area A_r / A_a is 12%. The consequence is that the effective bond energy will be lower than the work of adhesion, both due to the incomplete contact and the elastic deformation of contacting asperities. Based on the elastic contact model [3,4] an effective bond energy of 0.009 J/m^2 is calculated for an work of adhesion of 0.1 J/m^2.

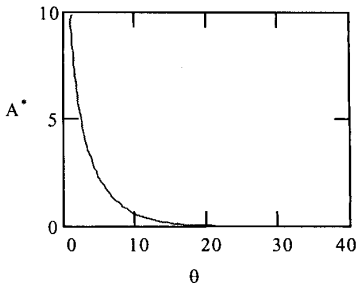

Figure 7: Normalized contact area A^* vs. the adhesion parameter θ, for equilibrium with zero applied (external) load.

PRESSURE TEST PROCEDURE

Model remarks

From the fabricated structure shown in fig. 4 it becomes clear that a relatively deep channel is etched into the silicon, leaving a thin silicon channel bottom.
Thus, beside the Pyrex, the silicon will bend during pressurization as well. This bending will occur mainly at the thin channel bottom, because there the bending stiffness is approximately 15 times lower than that of the unetched part of the silicon. The bending of the channel bottom in itself does not alter the calculations. However, some of the stresses caused by that bending will be transferred along the channel walls to the point where the channel walls and the Pyrex touch. This will somewhat affect the pressure at which the bond opens. Because of the thin channel bottom, it is thought that this effect will be negligible and it will therefore be neglected.

Measurement setup

For the pressure measurements a Spectroflow 400 solvent delivery system (Kratos, Germany) with a pressure range from 0 to 400 bar and a flow rate from 0 to 4.99 ml/min was used. The pump was equipped with a Bourbon pressure gauge with electro-optical converter and a 3 digit display in bar.
Providing a flow to a high resistance fluid recirculation loop resulted in a pressure drop. Splitting the loop at the high pressure side created a static pressurized liquid source. The flow resistance consisted of fused silica capillaries (75 μm ID, 55 cm long and 100 μm ID, 32 cm long). The pressure was varied by changing the flow rate in the loop. Static pressure to the chip was applied by connecting the capillaries that were glued on both sides of the channel to the high pressure split from the source.

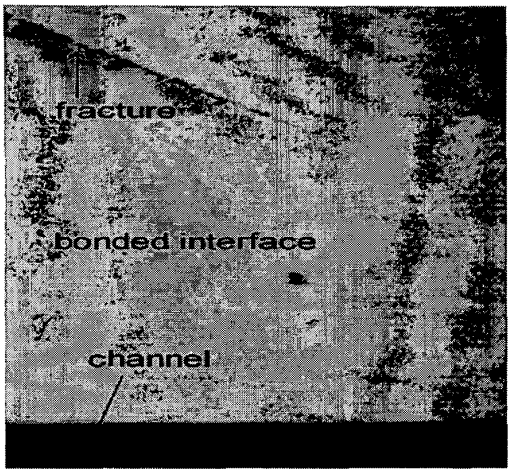

Figure 8: Interface after pressure test (top view). It is clear that there is some distance between the onset of the crack and the channel edge. Thus the interface must have opened.

Measurement procedure

For each channel the pressure was increased in steps that depended on the expected maximum pressure. For pressures that were expected from theory to lie below 15 bars, the pressure was increased by 1 bar; above, the step size was 2 bars. After each step the pressure was allowed to stabilize.

Essential for the comparison of measurements and theory is that failure of the channel occurs according to mechanism B. Thus the bond interface should crack before the glass breaks, as shown in fig. 1B. It turned out that for all measurements mechanism B was indeed the leading mechanism. In fig. 8 this becomes clear because the crack in the Pyrex starts at a certain distance from the channel edge. Evidence for the fact that the interface indeed was opened was given by fluid flowing out of the glass crack. Consequently, the developed theory can be applied to the measurements.

RESULTS

The results of the pressure tests are shown in fig. 9. Several conclusions can be drawn. First, the collapse pressure is smallest (9 bars) for the widest channel (2.0 mm). Secondly, the pressure increases for smaller channels. A graph (fig. 10) relating the maximum pressures and the reciprocal of the channel width squared shows that the predicted linear dependence of the maximum pressure on $1/w^2$ is correct, especially for lower pressures.

Deviations from the theory can be due to extra stresses in the silicon, as mentioned earlier. These, of course, will be more prominent at higher pressures, which could explain the deviations observed for such conditions in fig. 9. Thus, for a better evaluation of the

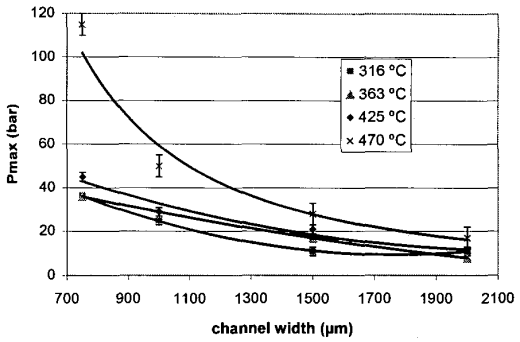

Figure 9: Maximum pressures for different channel widths

theory, thicker silicon wafers and more shallow channels should be used, so that really only the Pyrex bending is of influence. Another reason for deviations could be a nonuniform temperature distribution during annealing resulting in local bond strength variations.

Furthermore, it can be concluded from fig. 10 that the slope of the p_{max} versus $1/w^2$ curves depends on the anneal temperature. Because the modulus of elasticity and the Pyrex thickness are the same for all samples, this is due to a difference in bond strength. This is shown in fig. 10. The effective bond energy increases from 0.018 J/m^2 to 0.19 J/m^2 with the anneal temperature increasing from 310^{0}C to 470^{0}C (fig. 11). This increase in bond strength with temperature is explained in [9,10,11] by the chemical formation of stronger bonds during annealing.

The increase of the work of adhesion will increase the effective bond energy for the area already in contact. It will also lead to an increase in the effective bond energy by growth of the real contact area.

The wafer pair annealed at 310°C has an effective bond energy of about a factor two higher than the calculated pre-bond strength. This can be explained by the fact that the increase of bondstrengthening by hydrogen bond formation between silanol groups has already started at this temperature [9,10,11].

The effective bond energy at the lowest anneal temperature is 0.018 J/m^2. Using the elastic contact model and the measured roughness parameters, this implies a work of adhesion of 0.13 J/m^2. For the highest annealing temperature an effective bond energy of 0.19 J/m^2 was found, which corresponds to a work of adhesion of 0.44 J/m^2.

This is in agreement with the adhesion energies given for hydrophilic-hydrophilic wafer pairs in [10].

CONCLUSIONS

For pressurized microchannels, the relation between maximum pressure, channel geometry, materials elasticity and bond energy was investigated. An energy model was developed, which is substantiated by the

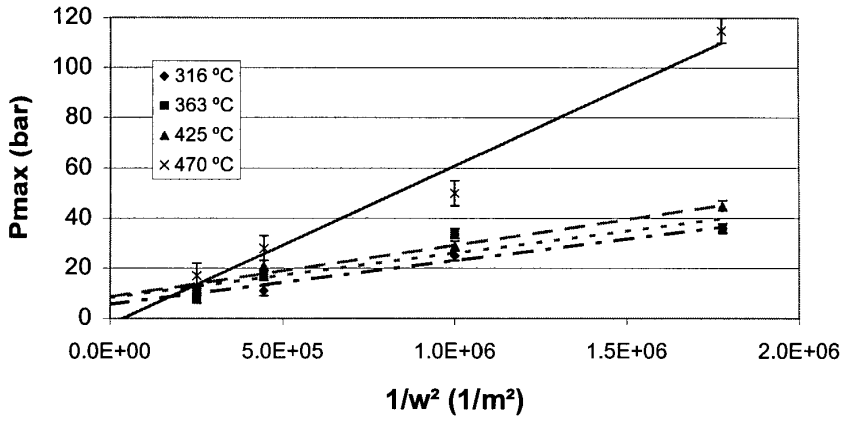

Figure 10: Maximum pressure vs. $1/w^2$. It can be concluded that the predicted linear dependence of the maximum pressures on the reciprocal of the channel width squared is correct.

measured yield pressures. The predicted linear dependence of the maximum pressures on the reciprocal of the channel width squared is correct. This gives a possibility to calculate the effective bond energy for fusion bonding of Pyrex to oxidized silicon. The effective bond energy increases from 0.018 J/m^2 to 0.19 J/m^2 for an annealing temperature increasing from 310°C to 470°C. Corrected for the influence of surface roughness this implies that the work of adhesion increases from 0.13 J/m^2 to 0.44 J/m^2.

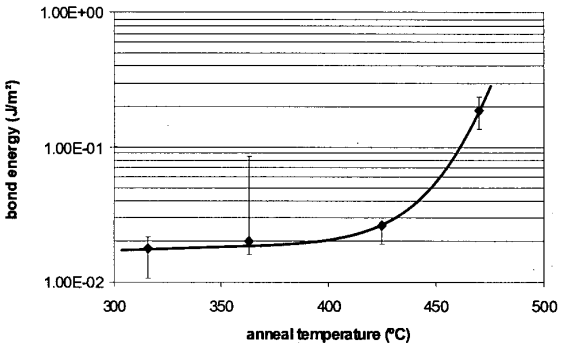

Figure 11: Effective bond energy for different annealing temperatures. The bond energy increases with increasing temperature.

ACKNOWLEDGEMENTS

The authors wish to thank the Dutch Technology Foundation STW for its support. This research was performed within the framework of the STW project "Hydrodynamic chromatography in integrated micro-machined separation systems", which is a cooperation of the University of Twente and the University of Amsterdam. Furthermore the authors are grateful to Meindert Dijkstra for polishing the Pyrex wafers.

REFERENCES

[1] N.F. Raley, J.C. Davidson, J.W. Balch, "Examination of glass-silicon and glass-glass bonding techniques for microfluidic systems", Proceedings of the SPIE 2639 (1995), p. 40-50.

[2] G. Ocvirk, E. Verpoorte, A. Manz, M. Grasserbauer, H.M. Widmer, "High performance liquid chromatography partially integrated onto a silicon chip", Anal. Methods and Instr. 2, no.2 (1995), p. 74-82.

[3] C. Gui, M. Elwenspoek, N.R. Tas, and J.G.E. Gardeniers, "The surface adhesion parameter: a measure for wafer bondability", Proc. IEEE MEMS Workshop 1999, Orlando Florida, USA, Jan. 17-21 1999, pp. 290-295.

[4] C. Gui, M. Elwenspoek, N.R. Tas, and J.G.E. Gardeniers, "The effect of surface roughness on direct wafer bonding", J. Appl. Phys. 85 (1999), pp. 290-295.

[5] J.M. Gere, S.P. Timoshenko, "Mechanics of Materials", Third SI Edition, Chapman & Hall, 1991.

[6] J.A. Greenwood and J.B.P.Williamson, "Contact of nominally flat surfaces", Proc. of the Royal Soc. of London, vol. A295, 1966, pp.300-319

[7] D. Maugis, "On the contact and adhesion of surfaces", J. Adhesion Sci. Technol. 10, no. 2 (1996), p. 161-175.

[8] K.N.Q. Fuller, D. Tabor, "The effect of surface roughness on the adhesion of elastic solids", Proc. R. Soc. London, Vol. A. 345, 1975, pp. 327-342.

[9] R. Stengl, T. Tan, U. Gösele, "A model for the Silicon Wafer Bonding Process", Jap. J. of Appl. Phys., vol. 28, no. 10, Oct. 1989, pp. 1735-1741.

[10] W.P. Maszara, G. Goetz, A. Caviglia, J.B. McKitterick, "Bonding of silicon wafers for silicon-on-insulator", J. Appl. Phys. 64 (1988), p. 4943-4950.

[11] G. Kissinger, W. Kissinger, "Void-free silicon-wafer-bond strengthening in the 200-400 °C range", Sensors and Actuators A 36 (1993), p. 149-156.